

Influence of hydrogen on electron-phonon coupling and intrinsic electrical resistivity in zirconium: a first-principles study

Qicheng Tang,^{1,2,*} L. A. Svyatkin,³ and I. P. Chernov³

¹Department of Physics, Zhejiang University, No.38, Zheda Road, Hangzhou 310027, China

²School of Science, Westlake University, No.18, Shilongshan Road, Hangzhou 310024, China

³Tomsk Polytechnic University, No.30, Lenina Avenue, Tomsk 634050, Russia

(Dated: December 14, 2024)

The paper presents the first-principle calculation of the electron-phonon coupling and the temperature dependence of the intrinsic electrical resistivity of the zirconium-hydrogen system with various hydrogen concentrations. The nature of the anomalous decrease in the electrical resistivity of the Zr-H system with the increase of hydrogen concentration (at the high concentrations of $H/Zr > 1.5$) was studied. It was found that the hydrogen concentration, where the resistivity starts to decrease, is very close to the critical concentration of the $\delta - \varepsilon$ phase transition. It was shown that the tetragonal lattice distortion due to the $\delta - \varepsilon$ phase transition of the Zr-H system eliminates imaginary phonon frequencies and the strong electron-phonon coupling of the δ phase and, as a result, leads to the reduction of the electrical resistivity of the Zr-H system at a high hydrogen concentration.

PACS numbers: 63.20.Kr, 64.70.Kb, 71.20.Be, 72.15.-v

I. INTRODUCTION

The features of the metal-hydrogen interaction have extensively been studied over many years¹⁻³. The addition of hydrogen in metals leads to the change in its mechanical, transport, magnetic and other properties caused by the electron density redistribution and the change of the phonon structure and electron-phonon coupling. To make the properties of metal-hydrogen system controllable, it's essential to study the relation between metal-hydrogen interaction and the change in different properties of metals. One of the most interesting changes is that the hydrogen absorption leads to the significant increase of the superconducting critical temperature which was firstly found in the thorium⁴ and in the palladium⁵.

The electron-phonon coupling (EPC) known as an important physical process in metal superconductivity, it's also important for studying its other transport properties, in particular, electrical resistance. The measurement of the electrical resistivity can help to identify the type of defects (in particular impurities) and their concentration in a real material. Moreover, the date of electrical resistivity is also helpful for understanding the heat conduction and other thermal properties of metals. An interesting fact observed in the experiments is the reduction of the electrical resistivity in some hydrogen-metal systems at very high H concentrations. In the Pd-H system this reduction occurs at the concentration $H/Pd \approx 0.71$ ⁶ at 300 K and $H(D)/Pd \approx 0.75$ ⁷ at 298 K, in the Zr-H system it occurs at the concentration $H/Zr \approx 1.6$ ⁸ at 300 K. It is assumed that the reduction of the electrical resistivity ρ at a high H concentration is related to the phase transition of the Pd-H⁶ and Zr-H⁸ systems.

This work focuses on the study of the Zr-H system. Zr-based alloys are extensively used as structural materials of active zones of light water reactors, since Zr has a low thermal-neutron absorption cross section, good corrosion resistance and strength characteristics. Hydrogen is ac-

tively accumulated in the materials during the reactor operation and causes their corrosion and degradation of their mechanical properties⁹⁻¹¹. To study the influence of hydrogen on the mechanical properties of zirconium-based alloys, the knowledge of the atomic structure of the zirconium-hydrogen system is necessary. It was shown in the experimental and theoretical works that at low H concentrations, the Zr-H system has a hexagonal close packed (HCP) structure and H atoms are located at tetrahedral interstitial sites¹⁶⁻¹⁹. At high H concentrations ($1 \leq H/Zr \leq 2$), the Zr-H system has a face-centered cubic (FCC) or face-centered tetrahedral (FCT) structure^{11,20-23}. The transition from the δ phase (FCC structure) into the ε phase (FCT structure, $c < a$) is investigated in the works^{21,23-27}, and it is known that the critical H concentration of this phase transition is located at $x \geq 1.5$. It has been reported that there is a strong reduction in the electron state density at Fermi level due to the $\delta - \varepsilon$ phase transition (for ZrH_2 this reduction achieves 0.5 states/eV per unit cell²⁷). The electron-driven mechanisms of $\delta - \varepsilon$ phase transition in Zr-H system with $1 \leq x \leq 2$ have been investigated in the works^{22,27-31}, but, to our knowledge, there is still no the *ab initio* study of the correlation between the phase transition and electron-phonon coupling in the Zr-H system.

The electrical properties of Zr-H system was measured experimentally for the different purposes, like for the research of the hydrogen kinetics¹², the thermal properties¹³, and the isotope effect^{14,15} e.t.c. Unlike the Pd-H system, the phonon distribution in the Zr-H system can be described by the linear response theory since the hydrogen atoms in Zr behave like the "Einstein" oscillators (independent simple harmonic oscillators). This makes the first-principle calculation of EPC in the Zr-H system possible within the density functional perturbation theory (DFPT). In present work, the H concentration influence on the electron-phonon coupling and intrin-

sic electrical resistivity of Zr is theoretically studied. The electron-phonon coupling was analyzed by means of the Eliashberg function $\alpha^2 F(\omega)$ and the Eliashberg transport function $\alpha_{tr}^2 F(\omega)$. To clarify the relevance between the $\delta - \varepsilon$ phase transition and the reduction of the electrical resistivity, the influence of the tetragonal lattice distortion on the electron-phonon coupling of ZrH₂, as an example, was investigated. Before the calculation of the electron-phonon coupling, we have determined the lattice structure of the Zr-H system, and the results are discussed in Appendix.

II. METHODOLOGY AND COMPUTATIONAL DETAILS

All calculations in our work were carried out from first-principle within the density functional theory (DFT) and DFPT using the optimized norm-conserving Vanderbilt pseudopotential method (ONCVSP)³², as implemented in the ABINIT³³ code. To describe the exchange and correlation effects, the generalized gradient approximation in the form of Perdew, Burke and Ernzerhof (GGA-PBE)³⁴ was used. The cut-off energy for the plane wave basis was set to 30 Ha in the structural optimization and relaxation and 40 Ha in the electronic structure calculation and linear response calculation. To describe the occupation of electron levels, the temperature smearing method of ‘‘cold smearing’’³⁵ with a broadening of 0.001 Ha (about 316 K) was adopted, and the cut-off energy of smearing function was set to 0.5 Ha. For structural optimization, the Broyden-Fletcher-Goldfarb-Shanno minimization (BFGS)³⁶ was adopted. The atoms in the system considered were assumed to be in the equilibrium configuration when the force on each atom was below 10^{-4} Ha/Borh.

The present calculations were performed for ZrH_{0.5}, ZrH, ZrH_{1.25}, ZrH_{1.5}, ZrH_{1.75}, ZrH₂ and pure Zr. In our calculations we considered three possible structures: HCP, FCC, and FCT, with the H atoms occupying all tetrahedral (T) or all octahedral (O) sites. To carry out the structural optimization and relaxation of the system considered, the supercell with 4 Zr atoms was adopted, and the k-meshes were chosen as $13 \times 13 \times 4$ for HCP structure and $14 \times 14 \times 14$ for FCC, FCT structures. In the electronic structure calculations (including the calculation of a band structure and the electronic density of states (EDOS)) for the ZrH₂ δ and ε phases, the k-meshes of $32 \times 32 \times 32$ and $30 \times 30 \times 34$, respectively, were adopted. In linear response calculations, for pure Zr and ZrH the supercell with 2 Zr atoms was adopted, the k-mesh of $14 \times 14 \times 10$ and the q-mesh of $7 \times 7 \times 5$ were chosen. For ZrH_{1.25}, ZrH_{1.5}, ZrH_{1.75} the supercell with 4 Zr atoms was adopted, the k-mesh of $14 \times 14 \times 14$ and the q-mesh of $7 \times 7 \times 7$ were chosen. For ZrH₂ the primitive cell was used, the k-mesh of $24 \times 24 \times 24$ and the q-mesh of $12 \times 12 \times 12$ were chosen.

By means of DFPT within the linear response the-

ory, the first-order perturbation potentials $\Delta_{qv}v$ for a phonon with frequency ω_{qv} (crystal momentum \mathbf{q} and branch index v) were calculated. Then they were used in the calculation of the electron-phonon matrix elements as $g_{ij\nu}(\mathbf{k}, \mathbf{q}) = \langle \psi_{i\mathbf{k}+\mathbf{q}} | \Delta_{qv}v | \psi_{j\mathbf{k}} \rangle$. More details about the theoretical methods can be found in the review by Feliciano³⁷. The Eliashberg function³⁸, which measures the contribution of the phonons with frequency ω to scattering processes of the electrons at the Fermi level, was calculated in terms of the phonon linewidths γ_{qv} ,

$$\alpha^2 F(\omega) = \frac{1}{2\pi N(\varepsilon_F)} \sum_{qv} \sum_{ijk} \frac{\gamma_{qv}}{\omega_{qv}} \delta(\hbar\omega - \hbar\omega_{qv}), \quad (1)$$

where $N(\varepsilon_F)$ is the EDOS per atom and spin at the Fermi level ε_F . The linewidth γ_{qv} is written by electron-phonon matrix elements $g_{ij\nu}(\mathbf{k}, \mathbf{q})$:

$$\gamma_{qv} = 2\pi\omega_{qv} \sum_{ijk} |g_{ij\nu}(\mathbf{k}, \mathbf{q})|^2 \delta(\varepsilon_{j\mathbf{k}} - \varepsilon_F) \delta(\varepsilon_{i\mathbf{k}+\mathbf{q}} - \varepsilon_F). \quad (2)$$

The strength of $\alpha^2 F(\omega)$ is described by the parameter

$$\lambda = 2 \int_0^\infty \frac{d\omega}{\omega} \alpha^2 F(\omega), \quad (3)$$

which is called the electron-phonon coupling constant.

For the calculation of transport properties, the tetrahedron smearing method³⁹ was adopted. The Eliashberg transport function⁴⁰, which is used to describe the influence of the electron-phonon scattering on transport properties, and additionally considers the efficiency factor of electronic transport $\eta_{\mathbf{k},\mathbf{q}}$, is calculated as follows

$$\alpha_{tr}^2 F(\omega) = \frac{1}{N(\varepsilon_F)} \sum_{qv} \sum_{ijk} \eta_{\mathbf{k},\mathbf{q}} |g_{ij\nu}(\mathbf{k}, \mathbf{q})|^2 \delta(\varepsilon_{n\mathbf{k}} - \varepsilon_F) \times \delta(\varepsilon_{m\mathbf{k}+\mathbf{q}} - \varepsilon_F) \delta(\hbar\omega - \hbar\omega_{qv}), \quad (4)$$

where an efficiency factor $\eta_{\mathbf{k},\mathbf{q}} = 1 - \frac{\mathbf{v}_{i\mathbf{k}+\mathbf{q}} \cdot \mathbf{v}_{j\mathbf{k}}}{\langle \mathbf{v}^2 \rangle}$ has been introduced in the terms of the electron velocity $\mathbf{v}_{j\mathbf{k}}$ in the state $|\psi_{j\mathbf{k}}\rangle$, and here $\langle \mathbf{v}^2 \rangle$ is the average square of the Fermi velocity. The strength of $\alpha_{tr}^2 F(\omega)$ is described by the parameter

$$\lambda_{tr} = 2 \int_0^\infty \frac{d\omega}{\omega} \alpha_{tr}^2 F(\omega), \quad (5)$$

which is called the transport constant. For a metal, the electrical resistivity can be calculated by solving the Boltzmann equation in the lowest-order variational approximation (LOVA)⁴¹, and written in terms of $\alpha_{tr}^2 F(\omega)$ as follows

$$\rho(T) = \frac{\pi\Omega k_B T}{N(\varepsilon_F) \langle \mathbf{v}^2 \rangle} \int_0^\infty \frac{d\omega}{\omega} \frac{x^2}{\sinh^2 x} \alpha_{tr}^2 F(\omega), \quad (6)$$

where $x = \hbar\omega/(2k_B T)$ and Ω is the unit cell volume.

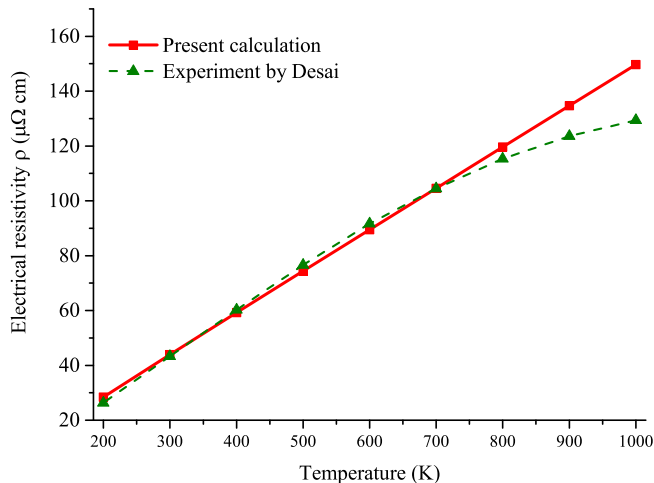


FIG. 1. The temperature dependence of the electrical resistivity $\rho(T)$ of pure Zr.

III. RESULTS AND DISCUSSION

A. Electron-phonon coupling and electrical resistivity of Zr-H system

Firstly we present the calculated temperature dependence of the Zr electrical resistivity and experimental results⁴² in Fig. 1. It can be seen that the theoretical curve is close to the experimental data for temperature up to ~ 800 K. At a temperature above ~ 800 K, a significant deviation of the calculated dependence on the experimental results is observed. This situation is caused by two factors. Firstly, at the temperature of 823 K the transformation of the α phase with a HCP structure into the β phase with a body-centered cubic (BCC) structure is observed¹¹. Secondly, the harmonic approximation which is used in the present work to describe the EPC is incorrect at high temperature. We did not investigate the electrical resistivity at a temperature below ~ 200 K, since in this case, in addition to the electron-phonon scattering, the size effects, electron-electron scattering, scattering on impurities, etc. give significant contributions to the electrical resistance⁴¹.

The calculated electrical resistivity ρ of the ZrH_x system depending on the H concentration at 300 K is shown together with the experimental data^{8,13,15} in Fig. 2. We also calculated this dependence at the typical operating temperature of the nuclear reactor (650 K). Unfortunately, in the literature there are no experimental data for this temperature. Since at a temperature of 650 K the harmonic approximation allows the correct calculation of the electrical resistance, the calculated results have practical importance. It can be seen from Fig. 2 that the behavior of the function $\rho(x)$ is the same at both temperature values, though at the higher temperature the function $\rho(x)$ is changed more sharply due to a stronger lattice vibration. According to both our and the experi-

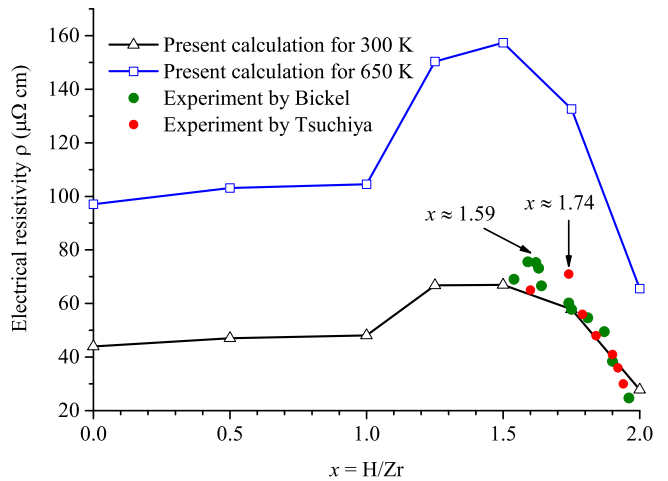


FIG. 2. The dependence of the electrical resistivity $\rho(x)$ of the Zr-H system on a hydrogen concentration. The electrical resistivity was calculated in $[\bar{1}2\bar{1}0]$ direction for pure Zr and $\text{ZrH}_{0.5}$ (both have a HCP structure) and in $[100]$ direction for zirconium hydrides (at the hydrogen concentration $x \geq 1$).

mental results, the reduction in the electrical resistivity is begun at the H concentration $x_c \sim 1.5$ and at the H concentration $x \geq 1.9$ zirconium hydrides become a better electrical conductor than pure Zr.

It should be noticed that the concentration x_c is close to the concentration of the $\delta - \epsilon$ phase transition of the Zr-H system. The δ and ϵ phases have different values of the lattice parameter relation c/a . In Fig. 3, we present the dependence of the lattice parameters c and a on the H concentration in zirconium hydrides. It can be seen that, with the H concentration increasing the parameter a is increased, while the parameter c is decreased and, as a consequence, the value of the relation c/a is decreased. The lattice parameters c and a become equaled at the

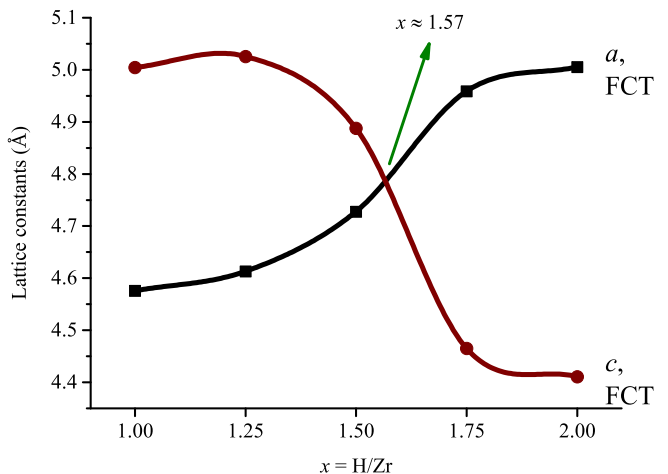


FIG. 3. The dependence of the lattice constants on the H concentration in the zirconium hydride.

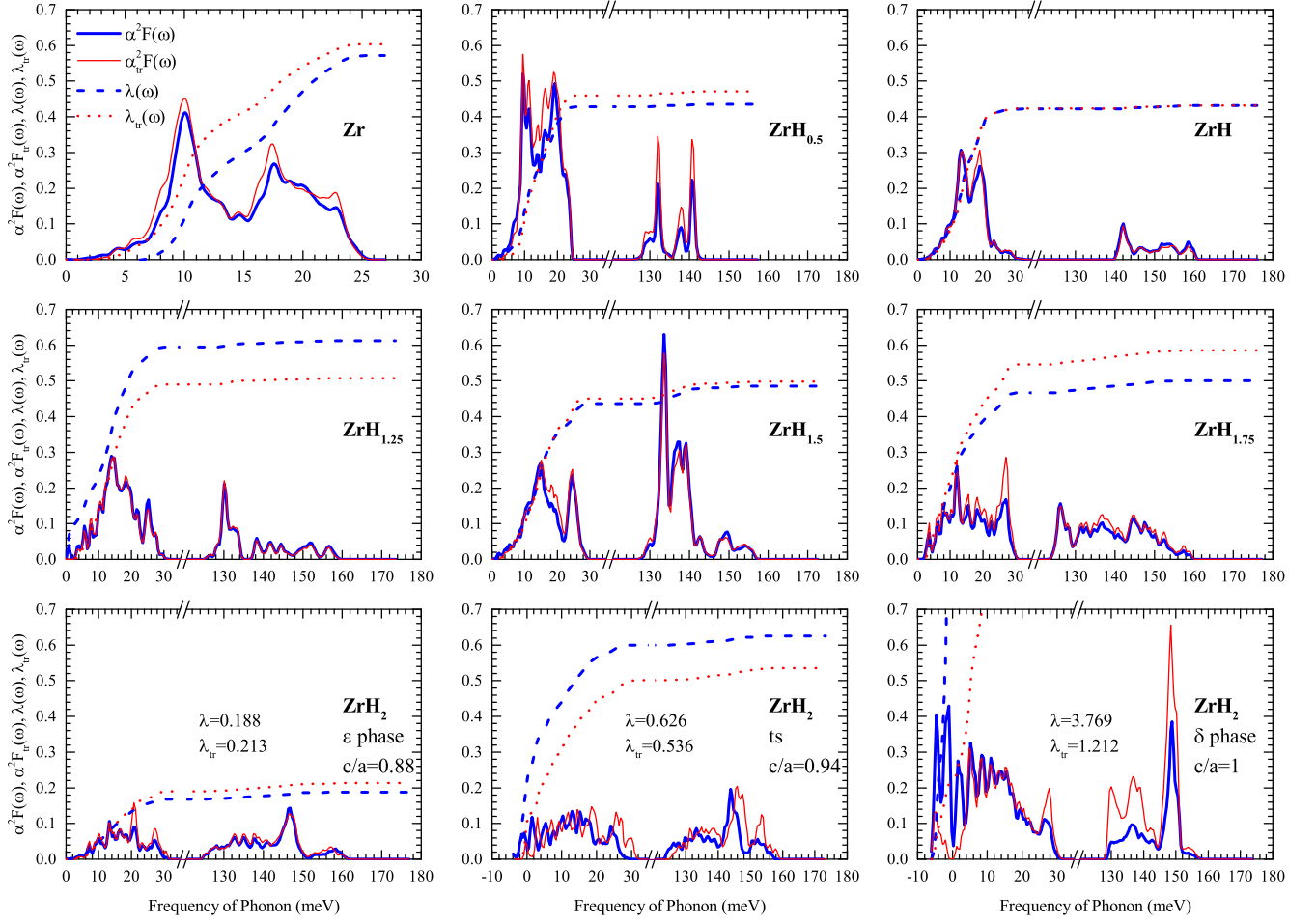


FIG. 4. The calculated Eliashberg function $\alpha^2 F(\omega)$, Eliashberg transport function $\alpha^2 F_{tr}(\omega)$ and their strength electron-phonon coupling constant λ and transport constant λ_{tr} for pure zirconium, $ZrH_{0.5}$, ZrH , $ZrH_{1.25}$, $ZrH_{1.5}$, $ZrH_{1.75}$ and ZrH_2 .

concentration $x \approx 1.57$ which is close to the experimental results of the $\delta - \varepsilon$ phase transition ($x \approx 1.6$)²³ and the concentration x_c . Thus, we assume that the observed behavior of the H concentration dependence of the electrical resistivity is related to the lattice tetragonal distortion in zirconium hydride. This relation will be discussed in detail in Sec. III B.

Further, we focus on the EPC in the Zr-H system. The calculated Eliashberg function $\alpha^2 F(\omega)$, Eliashberg transport function $\alpha^2 F_{tr}(\omega)$ and their strength electron-phonon coupling constant $\lambda(\omega)$ and transport constant $\lambda_{tr}(\omega)$ for Zr-H system with various H concentrations are shown in Fig. 4. The calculation value of $\lambda = 0.54$ for pure Zr indicates quite a strong electron-phonon coupling that is typical for transition metals due to the large effective mass of its d -electrons⁴³. A good agreement between the calculated resistivity and the experimental data allows us to conclude that the calculated spectra of $\alpha^2 F_{tr}(\omega)$ are credible.

It can be seen from Fig. 4 that the Eliashberg function and Eliashberg transport function are similar in shape, and the difference between the value of λ_{tr} and λ does

not exceed 17% in all the stable structures of the ZrH_x system. So, we can conclude that the efficiency factor μ , which gives a preferential weight from the backscattering process, has a small contribution on the electron-phonon scattering process for the Zr-H system⁴¹. It should be noticed that the difference between λ_{tr} and λ is very small in ZrH , $ZrH_{1.5}$ and ZrH_2 . In the cases of $ZrH_{1.25}$ and $ZrH_{1.75}$, which were not observed in the experiment, this difference is observable, which indicates a Fermi surface nesting which is related to the instability of these systems. Therefore, we will discuss below only the ZrH , $ZrH_{1.5}$ and ZrH_2 , which correspond to the experimentally observed γ , δ and ε zirconium hydride phases. In addition, it can be seen from the case of the unstable structures of ZrH_2 with $c/a = 0.94$ and $c/a = 1$ that the electron backscattering weakens the strong coupling. In particular, the system is not able to hold the strong EPC, since the strong coupling leads to the instability of the system. As a result, the system transforms into a new structure with a weaker coupling. It seems that there is a relevance between the electron backscattering and the phase transition in the Zr-H system. Specially, there

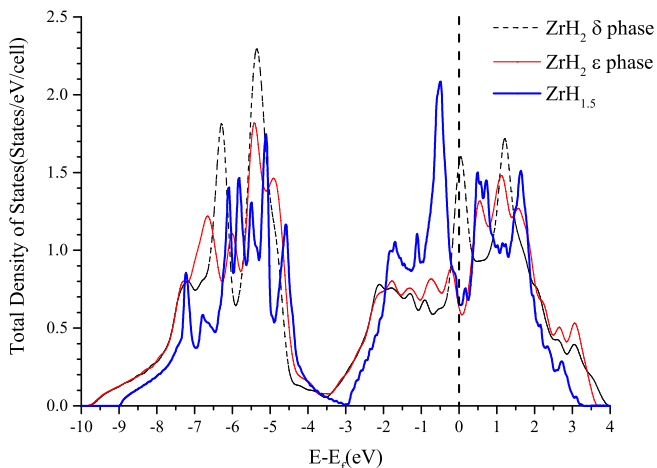


FIG. 5. The total EDOS in ZrH_2 δ , ϵ phases and $\text{ZrH}_{1.5}$. The Fermi level is set to the zero point.

is a significant difference between $\alpha^2 F(\omega)$ and $\alpha_{tr}^2 F(\omega)$ in δ - ZrH_2 due to the electron backscattering, which may cause a strong Fermi surface nesting⁴⁴ and a phase transition. It is clearly seen for ZrH_2 that the decrease in the value of c/a from 1 to 0.88 leads to the rise of the relation λ_{tr}/λ from 0.32 to 1.14. This means that the EPC becomes weaker due to the tetragonal distortion, and the strong Fermi surface nesting of the δ phase is receded. The weak EPC in ϵ - ZrH_2 can explain why ZrH_2 is a better conductor than pure Zr.

The contribution of H atoms to the electron-phonon scattering is also an interesting issue. It was found that the H-character phonons have a small contribution to λ and λ_{tr} in Zr-H system as shown Fig. 4. In particular, the contribution of the H-character phonon to λ is 2%, 10%, and 11% in ZrH, $\text{ZrH}_{1.5}$, and ZrH_2 , respectively. The small contribution of H atoms can be explained by the presence of strong Zr-H chemical bonds²⁷, which limits the H vibration modes in a small scale. This fact can also explain why the harmonic approximation describes correctly the phonon structure in Zr-H system. The contribution of the H-character phonon modes to EPC increases with the increasing of the H concentration.

B. Electron-phonon driven phase transition and reduction of electrical resistivity

In this section we will discuss in detail the influence of the tetragonal distortion of the FCC structure on the electrical properties of ZrH_2 . As we said, the instability of the FCC structure plays an important role in the reduction of the electrical resistivity, it leads to the $\delta - \epsilon$ phase transition and also makes the electron-phonon coupling weaken in the Zr-H system. There are three indications of the structural instability of the δ phase: the high pick of the EDOS at Fermi level, imaginary phonon frequencies and the extremely high value of the Fermi sur-

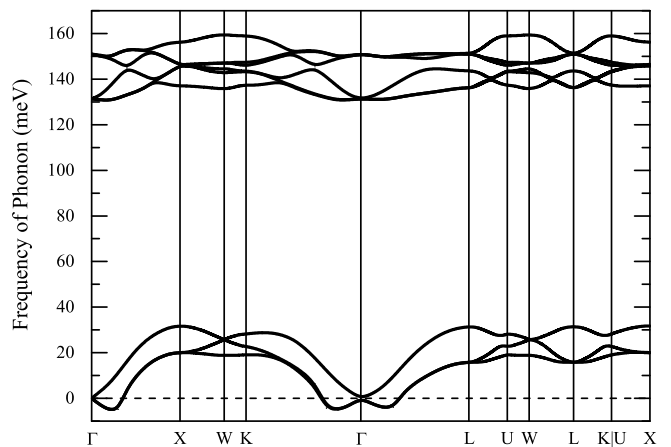


FIG. 6. The phonon spectrum of the ZrH_2 δ phase.

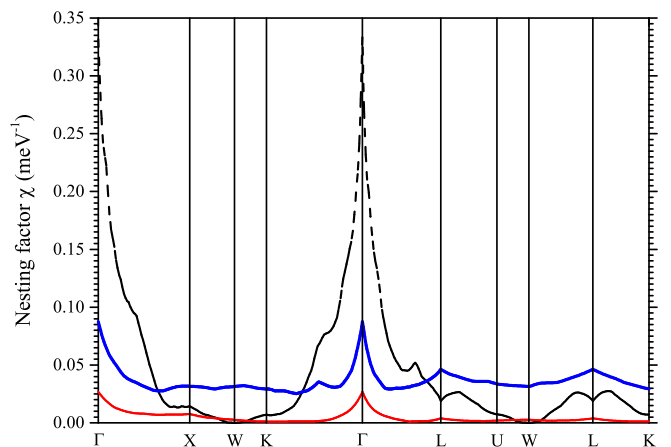


FIG. 7. The Fermi surface nesting factor for the ZrH_2 δ , ϵ phases and $\text{ZrH}_{1.5}$. The black dash line is the Fermi surface nesting factor of the ZrH_2 δ phase, the red solid line is the Fermi surface nesting factor of the ZrH_2 ϵ phase, and the blue solid line represents the Fermi surface nesting factor of $\text{ZrH}_{1.5}$.

face nesting factor, and they correspond to the electron-, phonon-, and electron-phonon- driven mechanisms of the tetragonal distortion in the Zr-H system. There are two main electron-driven mechanisms, the first is the splitting of the bands at the Fermi level in the $\Gamma - L$ direction due to Jahn-Teller effect^{22,26,27,29}, the second is the reduction of $N(\epsilon_F)$ by a shift in energy of the band along the $\Gamma - K$ direction^{25,27}. The key point is that the two electron-driven mechanisms lead to the reduction in $N(\epsilon_F)$ from the δ phase to the ϵ phase (Fig. 5). We can see that the high $N(\epsilon_F)$ splits to two peaks near the Fermi level through the $\delta - \epsilon$ phase transition, and the system obtains structural stability in this way. The phonon spectrum also shows the structural instability of the ZrH_2 δ phase. As shown in Fig. 6, in the $\Gamma - K$, $\Gamma - X$, $\Gamma - L$ directions the Zr-character phonon modes have the imaginary frequencies around the Γ point. In

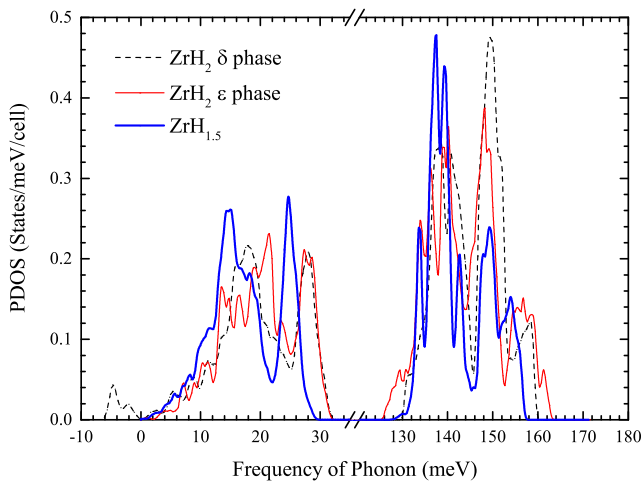


FIG. 8. The PDOS of the ZrH_2 δ , ϵ phases and $\text{ZrH}_{1.5}$.

consequence, in the $\Gamma - K$ and $\Gamma - L$ directions the signs of electron-driven mechanisms of phase transition were observed, so we can assume that the phase transition is related to the interaction between electrons and phonons.

According to Equation 6, there are three parameters which influence the electrical resistivity: the conduction electron concentration $n(\varepsilon_F) = N(\varepsilon_F)/\Omega$, the transport constant λ_{tr} and the average square of the Fermi velocity $\langle v^2 \rangle$. In Fig. 5 we also compare the EDOS between the ZrH_2 ϵ phase and $\text{ZrH}_{1.5}$ with the FCC(T) structure, since the $\text{ZrH}_{1.5}$ can be considered as the energetically stable configuration of the δ phase (the ZrH_2 δ phase is unstable). We can see that there is no significant difference of the EDOS at the Fermi level between the ZrH_2 ϵ phase and $\text{ZrH}_{1.5}$. In fact, the value of transport constant λ_{tr} of 0.498 for $\text{ZrH}_{1.5}$ is about 2.338 times higher than the value of 0.213 for ZrH_2 , and this is in a good agreement with the value of 2.4 for the ratio of $\rho(\text{ZrH}_{1.5})/\rho(\text{ZrH}_2)$. Thus, we conclude that the reduction in the electrical resistivity is defined by the change in λ_{tr} , the influences of the conduction electron concentration and the Fermi velocity are small and they equalize each other.

There are two factors which influence λ_{tr} : the Fermi surface nesting and the electron-phonon coupling matrix elements. To evaluate the Fermi surface nesting, we calculated the distribution of the nesting factor $\chi(\mathbf{q}) = \sum_{i,j\mathbf{k}} \delta(\varepsilon_{j\mathbf{k}} - \varepsilon_F) \delta(\varepsilon_{i\mathbf{k}+\mathbf{q}} - \varepsilon_F)$ in the reciprocal space as shown in Fig. 7. As we said, the strong nesting is the electron-phonon driven mechanism of the $\delta - \epsilon$ phase transition of the Zr-H system. It can be clearly seen that in the ZrH_2 δ phase, the nesting is strong around the Γ point in the $\Gamma - K$, $\Gamma - X$, $\Gamma - L$ directions where the imaginary phonon frequencies appear. It can also be found that the nesting factor has its maximum at the Γ point. It is interesting that the Γ point is like a singular point which is the center of imaginary phonon frequencies, but the Zr-character acoustic phonon frequencies at Γ point

are close to 0. The Zr-character acoustic phonon modes are following the “2+1” splitting⁴⁵, the frequencies of the two degenerate modes are imaginary, and the frequencies of split mode are positive. This may be caused by the fact that the nesting vector (points to the maximum of the nesting factor) $\mathbf{q} \rightarrow 0$ (Γ point), and the Γ point as a point with the highest degeneracy cannot be modified, so that the period-lattice-distortion and the charge-density modulation have not been observed in ZrH_2 , unfortunately. But the Fermi surface nesting behavior in ZrH_2 still can help us to understand the modification of the electron and phonon structures of the system, especially the changes around the Γ point. In particular, through the $\delta - \epsilon$ phase transition, the nesting factor χ not only strongly decreases around the Γ point, but also has a global reduction. If we compare the stable $\text{ZrH}_{1.5}$ and ZrH_2 , it can be seen that the nesting in $\text{ZrH}_{1.5}$ is stronger than in ZrH_2 . In particular, it can be seen that in the system the effect of the electron-phonon coupling on the electron transport is weakened due to the modification of the electronic structure, which leads to the decrease in the electrical resistance. Also, such a system with the strong Fermi surface nesting is unstable, and it may lead to a phase transition.

It is also important to investigate the influence of the electron-phonon coupling matrix elements, which indicates the strength of the single scattering process. To achieve this goal, we calculated the changes of the phonon density of states (PDOS) through the $\delta - \epsilon$ transition as shown in Fig. 8. It can be seen that the frequency range of the H-character optical phonon in both the ZrH_2 δ phase and $\text{ZrH}_{1.5}$ is narrower than in the ZrH_2 ϵ phase, and the gap between the acoustic and optical phonons in both the ZrH_2 δ phase and $\text{ZrH}_{1.5}$ is higher than in the ZrH_2 ϵ phase. At a high symmetry condition (cubic structure), phonon modes in system have a higher degeneracy, which leads to the high peak and narrow range of

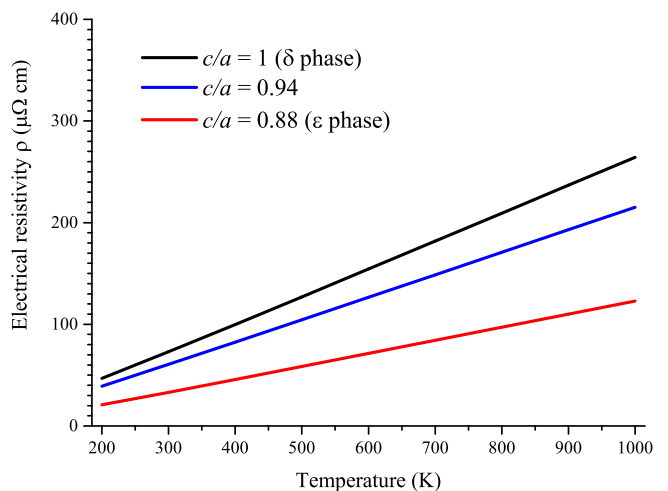


FIG. 9. The temperature dependence of the electrical resistivity in the ZrH_2 δ , ϵ phases and the “ts” state.

the H-character optical phonon frequency, and this might be a reason why the H-character optical phonon plays a more important role in the δ phase. The shapes of the PDOS and $\alpha^2F(\omega)$ are similar, in fact, $\alpha^2F(\omega)$ can also be seen as a modification of the PDOS with a weight from the electron-phonon coupling. It can be seen from Fig. 8 that the PDOS in the δ and ε phases have no significant difference, but the comparison of $\alpha^2F(\omega)$ between the δ and ε phases in Fig. 4 shows that the electron-phonon coupling in the δ phase is much stronger than in the ε phase. Thus, we can conclude that the electron-phonon coupling matrix elements play the defining role in the scattering process.

In addition, to clarify that the tetragonal distortion of a FCC structure is the reason for the decrease in the electrical resistance, we consider an imaginary transition state “ts” of ZrH₂ with the lattice volume and ratio c/a as the average of the δ and ε phases. The calculated results of the “ts” state show that this state has a structural instability weaker than the δ phase: the values of $\lambda = 0.626$ and $\lambda_{tr} = 0.536$ are lower than in the case of the δ phase, and higher than in the case of the ε phase. In the end, we show the calculated results of $\rho(T)$ for the ZrH₂ δ , ε phases and the “ts” state in Fig. 9. It can be clearly seen that the electrical resistivity of ZrH₂ decreases through the tetragonal distortion. In the δ phase the electrical resistivity is much higher, and the temperature dependence $\rho(T)$ is steeper than in the ε phase. It should be noticed that the results for the δ phase and “ts” state are not physical, because of the imaginary phonon frequencies. We can conclude that the high electrical resistivity in the δ phase is caused by its strong electron-phonon coupling, and it comes from the structural instability of the FCC structure. We can see that through the tetragonal distortion the imaginary phonon frequency and the strong electron-phonon coupling are eliminated. As a result, the stable state of the ε phase with the weak electron-phonon coupling strength is obtained, and it causes the reduction in the electrical resistivity of the ZrH_x system at a high hydrogen concentration ($x > 1.5$). In fact, the strong electron-phonon coupling in the δ phase can also be seen as a result of its high N_F . The high N_F provides a large number of backscattering electrons, and has a contribution to the strong Fermi surface nesting. Thus, we can conclude that the strong electron-phonon coupling has a significant relevance to the structural instability of the δ phase.

IV. SUMMARY AND CONCLUSIONS

In the present paper, the nature of the anomalous decrease in the electrical resistivity of the Zr-H system with increase of a hydrogen concentration (at H/Zr>1.5) has been studied within the framework of the electron density functional theory and the density functional perturbation theory, using the optimized norm-conserving Vanderbilt pseudopotential method. To understand the causes of

this reduction, we have analyzed the electron-phonon coupling in the Zr-H system by means of the Eliashberg function $\alpha^2F(\omega)$ and the Eliashberg transport function $\alpha_{tr}^2F(\omega)$. It has been shown that with the increasing of H concentration in Zr the change of the electron-phonon coupling strength is not strong except in ZrH₂. It has also been found that in the stable configuration of the Zr-H system the difference between $\alpha^2F(\omega)$ and $\alpha_{tr}^2F(\omega)$ is small, but strong in the ZrH₂ δ phase. It has been established that the significant difference between $\alpha^2F(\omega)$ and $\alpha_{tr}^2F(\omega)$ in the ZrH₂ δ phase is caused by the backscattering of electrons due to the strong Fermi surface nesting, which is one of the reasons why ZrH₂ transforms from the δ phase into the ε phase. It has been shown that the ZrH₂ δ phase has an extremely larger resistivity than the ε phase due to a strong electron-phonon coupling, which leads to the structural instability of the δ phase. The tetragonal lattice distortion due to the $\delta - \varepsilon$ phase transition of ZrH₂ eliminates imaginary phonon frequencies and the strong electron-phonon coupling.

ACKNOWLEDGMENTS

The research was carried out within the framework of the grant of the Program for Enhancing Competitiveness of Tomsk Polytechnic University.

Appendix: Structure of Zr-H system

Before the calculation of the electron-phonon coupling in the Zr-H system, we have determined the lattice structure of this system. It should be pointed out that, according to the results of previous works, there is ambiguity in the type of the atomic structure of ZrH_{0.5}. For ZrH_{0.5} the metastable state having a HCP structure with a low symmetry was identified by a transmission electron microscopy and first-principle calculations⁴⁶. However it was reported in the work⁹ that ZrH_{0.5} has the FCC structure in a high symmetry configuration. Hence, for ZrH_{0.5} we considered four configurations C1-C4 to study its structural stability as shown in Fig. 10.

Firstly we calculated the dissolution energy ΔE_H of hydrogen in zirconium

$$\Delta E_H = \frac{E_{Zr_aH_b} - aE_{Zr} - \frac{b}{2}E_{H_2}}{b}, \quad (A.1)$$

where $E_{Zr_aH_b}$, E_{Zr} and E_{H_2} are total energies of Zr_aH_b, pure HCP Zr (ground state) and a H₂ molecule, respectively. The ΔE_H of the various ZrH_x systems as the function of a H concentration are shown in Fig. 11. It can be seen from Fig. 11 that it is energetically most advantageous for the ZrH_x system to have the HCP(T) lattice structure at $x = 0.5$ and the FCT(T) structure at $1 \leq x \leq 2$. At the concentration of $1.5 \leq x \leq 1.75$, the dissolution energy of H in Zr with the FCT(T) structure exceeds its dissolution energy in Zr with the FCC(T)

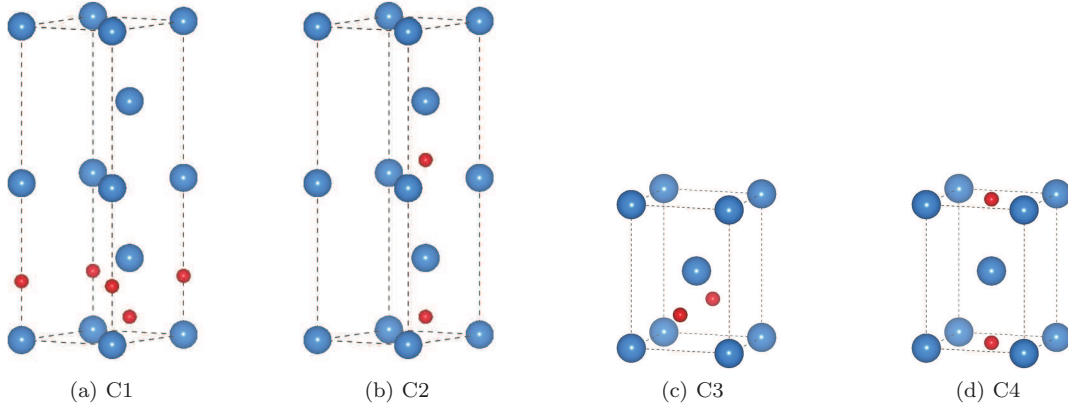


FIG. 10. The four configurations of $\text{ZrH}_{0.5}$ which were considered in our calculations.

TABLE I. The lattice parameters (a and c) for the calculated ZrH_x systems with H atoms located all at T or all at O sites.

System	Structure	a (Å)	c (Å)	c/a	Method	Reference
Pure zirconium	HCP	3.2346	5.1678	1.5976	GGA	Present work
		3.2317	5.1476	1.5928	Exp. (298K)	11
		3.213	5.159	1.605	GGA	9
		3.23	5.18	1.60	GGA	47
Zr_2H	HCP(T), C1	3.2603	5.3962	1.6551	GGA	Present work
		3.3	5.145	1.56	Exp. (293K)	46
		3.313	5.549	1.675	GGA	9
	HCP(T), C2(C3)	3.2433	5.4892	1.6925	GGA	Present work
		3.26	5.447	1.671	GGA	9
	FCT(T), C4	4.7597	4.4595	0.9369	GGA	Present work
4.676				GGA	9	
FCT(O), C5	4.4334	4.8431	1.0924	GGA	Present work	
	4.575			GGA	9	
ZrH	FCT(T)	4.5754	5.0045	1.0938	GGA	Present work
		4.5957	4.9686	1.081	Exp. (293K)	1
		4.61	5.04	1.093	GGA	31
$\text{ZrH}_{1.25}$	FCT(T)	4.6130	5.0252	1.0894	GGA	Present work
		4.79	5.20	1.086	GGA	31
$\text{ZrH}_{1.5}$	FCT(T)	4.7276	4.8874	1.0338	GGA	Present work
		4.65	4.96	1.067	Exp. (320K)	23
		4.62	4.83	1.046	GGA	31
$\text{ZrH}_{1.75}$	FCT(T)	4.9585	4.4651	0.9005	GGA	Present work
		4.9087	4.5220	0.9212	Exp. (118K)	22
		4.97	4.47	0.899	GGA	31
ZrH_2	FCT(T)	5.0053	4.4106	0.8812	GGA	Present work
		4.9808	4.4336	0.8901	Exp. (108K)	22
		4.975	4.447	0.894	Exp. (294K)	21
		4.982	4.449	0.893	Exp. (320K)	23
		5.021	4.432	0.883	GGA	27
	FCC(T)	4.8089			GGA	Present work
4.817				GGA	27	
4.82				GGA	47	
				LDA	29	

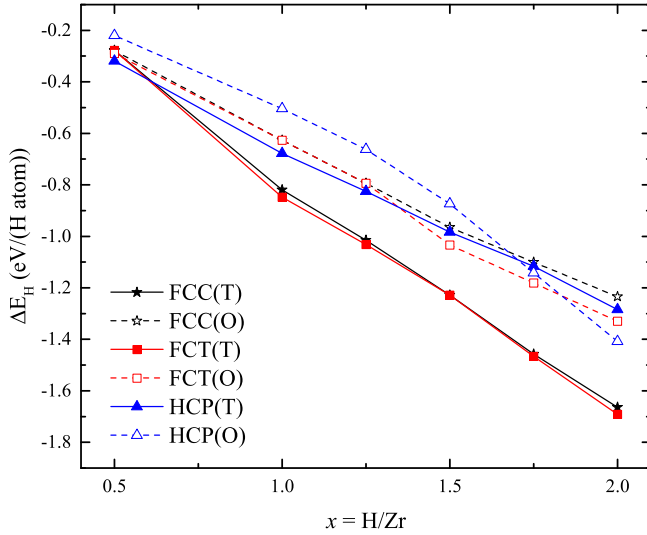


FIG. 11. The dissolution energy of hydrogen in zirconium as a function of the H concentration.

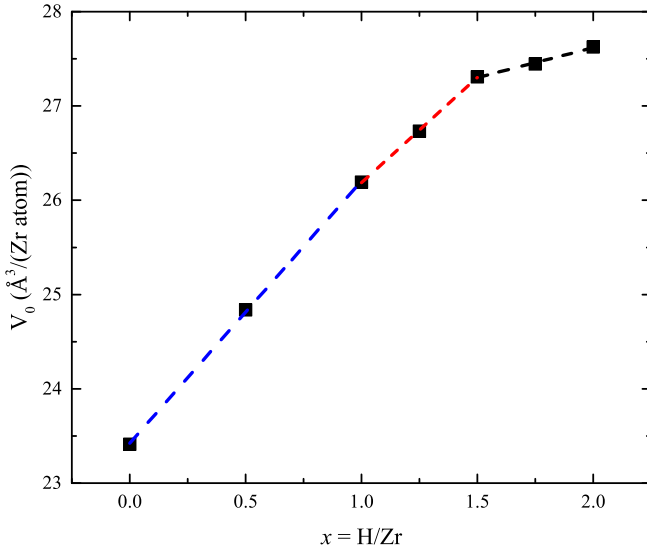
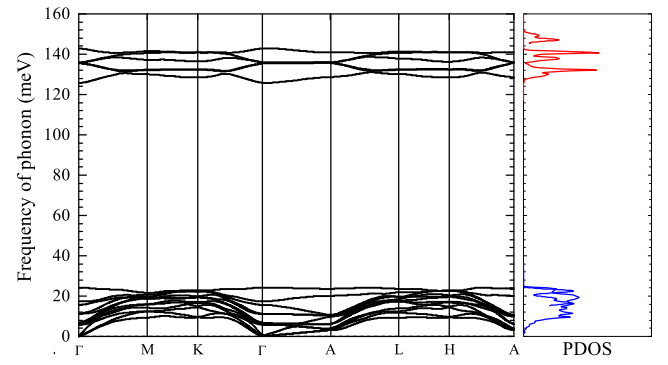
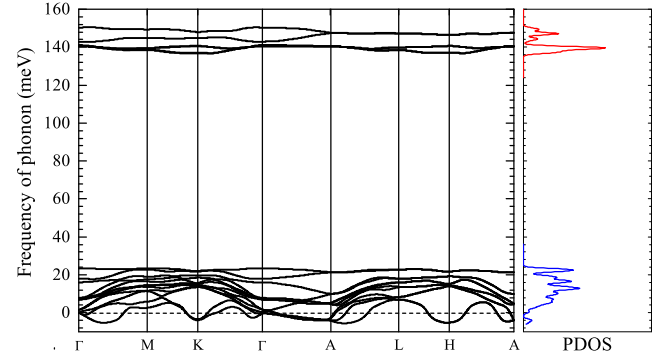


FIG. 12. The unit cell volume of the Zr-H system as a function of the hydrogen concentration. Here the three dash lines are the results of linear fitting in the ranges of $0 \leq x \leq 1$, $1 \leq x \leq 1.5$ and $1.5 \leq x \leq 2$.

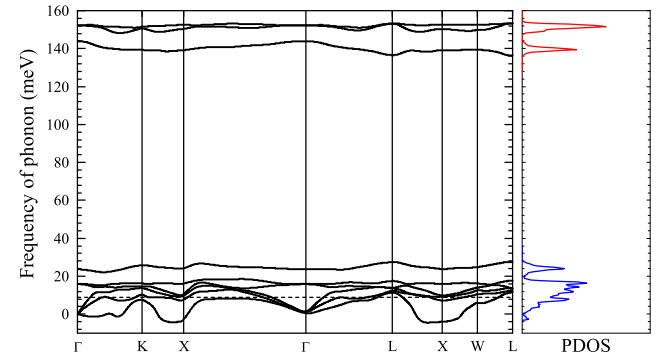
structure by an amount not exceeding 0.1 eV/(H atom). As a result, under external perturbations (for example, a radiation or a high temperature), the ZrH_x system can pass from the FCT structure to the FCC structure. It can also be seen that the H concentration dependence of the dissolution energy ΔE_H is linear partially with the slope coefficient of -0.900 ± 0.026 eV/(H atom). It should be pointed out that configuration C1 of $\text{ZrH}_{0.5}$, which is presented as the HCP(T) structure in Fig. 11, has the lowest total energy, however this energy is close to the total energies of configurations C3 and C4 with the FCT lattice (the difference in the total energy less than



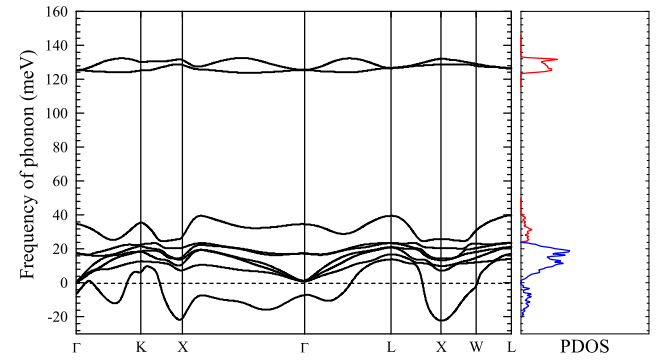
(a) HCP(T), C1



(b) HCP(T), C2



(c) FCT(T), C3



(d) FCT(O), C4

FIG. 13. The phonon spectra for Zr_2H having low symmetry configurations C1 and C2 with HCP(T) structure and high symmetry configurations C3 and C4 with FCT(T), and FCT(O) structures, respectively.

0.4 meV/(Zr atom)). Since the energy difference between the HCP and FCT structures of $\text{ZrH}_{0.5}$ is too small to determinate the stable structure, the phonon spectra of $\text{ZrH}_{0.5}$ with configurations C1-C4 were analyzed to study its structural stability (see Fig. 13). It can be clearly seen that the H location in Zr is important to structural stability of the Zr-H system: configurations C2-C4 have the imaginary phonon frequency, while configuration C1 does not.

The calculated lattice parameters (a and c) of pure Zr and the ZrH_x systems are shown in Table I and have very good agreement with the previous calculation results and experimental data^{1,9,11,21-23,27,46,47}. It is observed that the ratio c/a decreases with the increasing of

the H concentration in Zr, as in experiments^{22,23}. As the intrinsic electrical resistivity depends on the crystal volume (Equation 6), it is interesting to study a change in the crystal volume of the Zr-H system depending on the hydrogen concentration (see Fig. 12). This dependence has a linear character with the different slopes at the hydrogen concentration ranges of $0 \leq x \leq 1$, $1 \leq x \leq 1.5$ and $1.5 \leq x \leq 2$. The linear approximation by the least-squares method gives the lines with the slope coefficients of $2.78 \pm 0.04 \text{ \AA}^3/(\text{Zr atom})$ in the range of $0 \leq x \leq 1$, $2.23 \pm 0.04 \text{ \AA}^3/(\text{Zr atom})$ in the range of $1 \leq x \leq 1.5$ and $0.63 \pm 0.05 \text{ \AA}^3/(\text{Zr atom})$ in the range of $1.5 \leq x \leq 2$. The change of the slope in the dependence of the crystal volume on the hydrogen concentration is due to the phase transition in the Zr-H system.

-
- * tangqicheng@westlake.edu.cn
- ¹ W. M. Mueller, J. P. Blackledge, and G. G. Libowitz, *Metal hydrides* (Elsevier, 2013).
 - ² B. Sakintuna, F. Lamari-Darkrim, and M. Hirscher, *Int. J. Hydrog. Energy* **32**, 1121 (2007).
 - ³ Y. Fukai, *The metal-hydrogen system: basic bulk properties*, Vol. 21 (Springer Science & Business Media, 2006).
 - ⁴ C. Satterthwaite and I. Toepke, *Phys. Rev. Lett.* **25**, 741 (1970).
 - ⁵ T. Skoskiewicz, *Phys. Status Solidi A* **11** (1972).
 - ⁶ B. Geerken and R. Griessen, *J. Phys. F: Met. Phys.* **13**, 963 (1983).
 - ⁷ Y. Sakamoto, K. Takai, I. Takashima, and M. Imada, *J. Phys.: Condens. Matter* **8**, 3399 (1996).
 - ⁸ P. Bickel and T. Berlincourt, *Phys. Rev. B* **2**, 4807 (1970).
 - ⁹ F. Wang and H. Gong, *Int. J. Hydrog. Energy* **37**, 12393 (2012).
 - ¹⁰ A. Zieliński and S. Sobieszczyk, *Int. J. Hydrog. Energy* **36**, 8619 (2011).
 - ¹¹ E. Zuzek, J. Abriata, A. San-Martin, and F. Manchester, *Bulletin of Alloy Phase Diagrams* **11**, 385 (1990).
 - ¹² A. Grib, G. Khadzhay, B. Merisov, D. Vinogradov, and M. Tikhonovsky, *Int. J. Hydrog. Energy* **35**, 5442 (2010).
 - ¹³ B. Tsuchiya, M. Teshigawara, K. Konashi, and M. Yamawaki, *J. Alloy. Compd.* **330**, 357 (2002).
 - ¹⁴ M. Uno, K. Yamada, T. Maruyama, H. Muta, and S. Yamawaki, *J. Alloy. Compd.* **366**, 101 (2004).
 - ¹⁵ B. Tsuchiya, M. Teshigawara, K. Konashi, S. Nagata, T. Shikama, and M. Yamawaki, *J. Nucl. Sci. Technol.* **39**, 402 (2002).
 - ¹⁶ R. Khoda-Bakhsh and D. Ross, *J. Phys. F: Met. Phys.* **12**, 15 (1982).
 - ¹⁷ P. Narang, G. Paul, and K. Taylor, *Journal of the Less Common Metals* **56**, 125 (1977).
 - ¹⁸ O. V. Lopatina, L. A. Svyatkin, Y. M. Koroteev, and I. P. Chernov, *Phys. Solid State* **57**, 1719 (2015).
 - ¹⁹ L. Svyatkin, Y. M. Koroteev, and I. Chernov, *Phys. Solid State* **60**, 10 (2018).
 - ²⁰ G. Ackland, *Phys. Rev. Lett.* **80**, 2233 (1998).
 - ²¹ K. Niedźwiedz, B. Nowak, *et al.*, *J. Alloy. Compd.* **194**, 47 (1993).
 - ²² J. S. Cantrell, R. J. Bowman, and D. Sullenger, *J. Phys. Chem.* **88**, 918 (1984).
 - ²³ R. Bowman Jr, E. Venturini, B. Craft, A. Attalla, and D. Sullenger, *Phys. Rev. B* **27**, 1474 (1983).
 - ²⁴ H. Yakel, *Acta Crystallogr.* **11**, 46 (1958).
 - ²⁵ S. Kulkova, O. Muryzhnikova, and I. Naumov, *Phys. Solid State* **41**, 1763 (1999).
 - ²⁶ K. Miwa and A. Fukumoto, *Phys. Rev. B* **65**, 155114 (2002).
 - ²⁷ R. Quijano, R. de Coss, and D. J. Singh, *Phys. Rev. B* **80**, 184103 (2009).
 - ²⁸ M. Gupta, *Phys. Rev. B* **25**, 1027 (1982).
 - ²⁹ W. Wolf and P. Herzig, *J. Phys.: Condens. Matter* **12**, 4535 (2000).
 - ³⁰ P. Zhang, B.-T. Wang, C.-H. He, and P. Zhang, *Comp. Mater. Sci.* **50**, 3297 (2011).
 - ³¹ F. Wang and H. Gong, *Int. J. Hydrog. Energy* **37**, 9688 (2012).
 - ³² D. Hamann, *Phys. Rev. B* **88**, 085117 (2013).
 - ³³ X. Gonze, F. Jollet, F. A. Araujo, D. Adams, B. Amadon, T. Applencourt, C. Audouze, J.-M. Beuken, J. Bieder, A. Bokhanchuk, *et al.*, *Comput. Phys. Commun.* **205**, 106 (2016).
 - ³⁴ J. P. Perdew, K. Burke, and M. Ernzerhof, *Phys. Rev. Lett.* **77**, 3865 (1996).
 - ³⁵ M. Verstraete and X. Gonze, *Phys. Rev. B* **65**, 1 (2002).
 - ³⁶ R. Eitan, M. Mundt, and D. J. Tammor, *Phys. Rev. A* **83**, 053426 (2011).
 - ³⁷ F. Giustino, *Rev. Mod. Phys.* **89**, 015003 (2017).
 - ³⁸ P. B. Allen, *Phys. Rev. B* **6**, 2577 (1972).
 - ³⁹ D. Zaharioudakis, *Comput. Phys. Commun.* **157**, 17 (2004).
 - ⁴⁰ P. Allen, *Phys. Rev. B* **3**, 305 (1971).
 - ⁴¹ S. Y. Savrasov and D. Y. Savrasov, *Phys. Rev. B* **54**, 16487 (1996).
 - ⁴² P. D. Desai, H. M. James, and C. Y. Ho, *J. Phys. Chem. Ref. Data* **13**, 1097 (1984).
 - ⁴³ N. F. Mott, *Advances in Physics* **13**, 325 (1964).
 - ⁴⁴ V. H. Crespi and M. L. Cohen, *Solid State Commun.* **81**, 187 (1992).
 - ⁴⁵ P. Giannozzi, S. De Gironcoli, P. Pavone, and S. Baroni, *Phys. Rev. B* **43**, 7231 (1991).
 - ⁴⁶ Z. Zhao, J.-P. Morniroli, A. Legris, A. Ambar, Y. Khin, L. Legras, and M. Blat-Yrieix,

J. Microsc. **232**, 410 (2008).

⁴⁷ C. Domain, R. Besson, and A. Legris,
Acta Mater. **50**, 3513 (2002).